JOURNAL OF GEOPHYSICAL RESEARCH, VOL. 112, B09305, doi:10.1029/2006JB004719, 2007

Complex seismic anisotropy at the border of a very low velocity province at the base of the Earth's mantle

Yi Wang[1,2] and Lianxing Wen[1]

Received 26 August 2006; revised 8 April 2007; accepted 12 June 2007; published 18 September 2007.

[1] We constrain the anisotropy associated with a very low velocity province (VLVP) at the base of the Earth's mantle using the SKS and SKKS waves sampling the region. Our selected high-quality data sets consist of 415 SKS and 111 SKKS waveforms for 127 deep earthquakes recorded at distances between 90° and 150° by the seismic stations in three temporary broadband PASSCAL seismic arrays: the Kaapvaal seismic array (1997–1999), the Tanzania seismic array (1994–1995), and the Ethiopia/Kenya seismic array (1999–2001), as well as the permanent stations in the Global Seismographic Network. These seismic data provide good sampling coverage for some portion of the VLVP and its surrounding areas. Our results show, when the SKS or SKKS phases sample the regions away from the border of the VLVP (inside or outside the VLVP), the apparent splitting parameters inferred from the SKS phases are consistent with those inferred from the SKKS phases, and their variations strongly correlate with seismic stations but not with the exit points at the core-mantle boundary of these seismic phases. However, when the SKS or SKKS phases sample near the border of the VLVP, the apparent splitting parameters inferred from the SKS phases and SKKS phases are different, and their variations no longer correlate with seismic stations. These features indicate that part of the shear wave splitting for the seismic data sampling the border of the VLVP has to originate from deep mantle, most likely near the border of the VLVP. We assume that the anisotropy in the shallow mantle beneath seismic stations has a horizontal hexagonal symmetry axis and infer the splitting parameters associated with the shallow anisotropy beneath the seismic stations using the SKS and SKKS waveforms for the seismic data sampling the regions away from the border of the VLVP. We then obtain the splitting parameters associated with the lowermost mantle anisotropy using the SKS and SKKS waveforms corrected for the inferred shallow anisotropy beneath seismic stations, assuming that the medium in the lowermost mantle also has a horizontal hexagonal symmetry axis. Our results reveal a complex anisotropy pattern near the border of the VLVP. Such a complex anisotropy pattern may be explained by lattice-preferred orientation of anisotropic mantle aggregates aligned by a complex mantle flow near the VLVP margins. The complex flow pattern near the VLVP margins may indicate strong interactions between the VLVP, a compositional anomaly, and the surrounding normal mantle, and may provide an explanation to the concentration of some hot spots geographically near the borders of the VLVPs in the lowermost mantle.

Citation: Wang, Y., and L. Wen (2007), Complex seismic anisotropy at the border of a very low velocity province at the base of the Earth's mantle, *J. Geophys. Res.*, *112*, B09305, doi:10.1029/2006JB004719.

1. Introduction

[2] The "African Anomaly" is one of the two prominent low-velocity anomalies in the lower mantle [e.g., *Su et al.*, 1994; *Li and Romanowicz*, 1996; *Masters et al.*, 1996; *Grand et al.*, 1997; *van der Hilst et al.*, 1997; *Ritsema et al.*, 1999; *Wen et al.*, 2001; *Ni et al.*, 2002; *Ni and Helmberger*, 2003a, 2003b, 2003c; *Wang and Wen*, 2004, 2007; *He et al.*, 2006]. It has a very low velocity province (VLVP) as a broad base near the core-mantle boundary (CMB). The VLVP exhibits an "L-shaped" form changing from a north-south orientation in the South Atlantic Ocean to an east-west orientation in the Indian Ocean, occupying an area of about 1.8×10^7 km^2 [*Wang and Wen*, 2004]. Waveform modeling results suggest that the VLVP has rapidly varying thicknesses from 300 km to 0 km, steeply dipping edges, and a linear gradient of shear velocity reduction from −2%

[1]Department of Geosciences, State University of New York at Stony Brook, Stony Brook, New York, USA.
[2]Now at CGGVeritas, Houston, Texas, USA.

0148-0227/07/2006JB004719$09.00

(top) to −9 to −12% (bottom) relative to the Preliminary Reference Earth Model (PREM [*Dziewonski and Anderson*, 1981]) [*Wen et al.*, 2001; *Wen*, 2001; *Wang and Wen*, 2004]. These structural and velocity features unambiguously indicate that the VLVP is compositionally distinct, and can best be explained by partial melt driven by a compositional change, possibly produced early in the Earth's history [*Wen et al.*, 2001; *Wen*, 2001; *Ni and Helmberger*, 2003c; *Wang and Wen*, 2004]. A recent study further proposed that the VLVP may serve as an anchor to thermochemical plumes that give rise to three long-lived and relatively slowly moving hot spots in the South Atlantic and Indian Oceans and as source to the geochemical "DUPAL" anomaly [*Wen*, 2006]. The African Anomaly extends from the CMB continuously about 1300 kilometers into the mid-lower mantle with both sides of the anomaly dipping toward the apex beneath southern Africa [*Wang and Wen*, 2007]. The seismic data can best be explained by a shear velocity structure with an average velocity decrease of −5% in the base and of −2% to −3% in the mid-lower mantle, and a compressional velocity structure with a uniform S to P velocity perturbation ratio of 3:1 for the entire African Anomaly [*Wang and Wen*, 2007]. In addition, *Masters et al.* [2000] reported an anticorrelation of bulk sound velocity perturbation and shear velocity perturbation in the deep mantle beneath Africa. The density anomalies associated with the African Anomaly in the mid-lower mantle are also studied. For example, *Ishii and Tromp* [1999] and *Trampert et al.* [2004] suggested that the low-velocity anomaly in the lower mantle beneath Africa has a higher density, while *Lithgow-Bertelloni and Silver* [1998] and *Gurnis et al.* [2000] argued that positive density buoyancy is needed in the mid-lower mantle in order to explain the high topography and the uplift rate observed in southern Africa. Our recent study on these geometric and velocity features, however, suggests that the mid-lower mantle portion of the African Anomaly is an integral component of the VLVP and the African Anomaly is compositionally distinct and stable over geological time [*Wang and Wen*, 2007].

[3] Seismic anisotropy associated with the African Anomaly provides another valuable constraint on the dynamics of the anomaly. Seismic velocity anisotropy is a material property that seismic velocity varies with propagation and polarization directions. Two mechanisms have been proposed to generate seismic anisotropy: lattice-preferred orientation (LPO) of intrinsically anisotropic mineral aggregates [e.g., *Karato*, 1998] and shape-preferred orientation (SPO) of materials with contrasting elastic properties [e.g., *Kendall*, 2000]. For the LPO mechanism, the intrinsically anisotropic mantle mineral aggregates, such as olivine in the upper mantle, perovskite and magnesiowustite in the lower mantle and postperovskite in the lowermost mantle, are preferentially aligned along the maximal shearing direction of deformation-induced finite strain, causing seismic velocity to be higher along one particular direction than along the other two orthogonal directions [e.g., *Silver and Holt*, 2002]. For the SPO mechanism, anisotropy is generated when seismic waves propagate through a medium with materials of contrasting elastic properties alternately overlying each other [e.g., *Kendall and Silver*, 1996]. Over the past decade, seismic evidence has been accumulated to support the existence of anisotropy in the lowermost mantle. Previous studies of direct S, ScS and Sdiff phases suggest that there is vertical transverse isotropy (VTI, in which the medium has a vertical hexagonal symmetry) in the lowermost mantle associated with both the high-velocity regions, such as those beneath northern Pacific and Alaska [*Matzel et al.*, 1996; *Garnero and Lay*, 1997; *Fouch et al.*, 2001], Caribbean and central America [*Kendall and Silver*, 1996, 1998; *Lay et al.*, 1998; *Kendall*, 2000; *Garnero and Lay*, 2003; *Rokosky et al.*, 2004; *Maupin et al.*, 2005], Asia [*Thomas and Kendall*, 2002] and southern Indian [*Ritsema*, 2000], and the low-velocity regions, such as those beneath central Pacific [*Vinnik et al.*, 1995, 1998; *Ritsema et al.*, 1998; *Pulliam and Sen*, 1998; *Fouch et al.*, 2001; *Panning and Romanowicz*, 2004], southern Pacific [*Ford et al.*, 2006], and Africa [*Panning and Romanowicz*, 2004]. In addition, evidence for azimuthal anisotropy was reported in a localized region beneath central Pacific [*Russell et al.*, 1998, 1999], Central America [*Garnero et al.*, 2004; *Rokosky et al.*, 2006], and in the high-velocity regions beneath the Fiji-Tonga subduction region, North America and Eurasia [*Wookey et al.*, 2002; *Niu and Perez*, 2004; *Restivo and Helffrich*, 2006]. However, the anisotropy associated with the African Anomaly remains unclear.

[4] In this study, we jointly constrain seismic anisotropy in the shallow mantle beneath seismic stations and in the base of the African Anomaly using SKS and SKKS waveforms. In the following sections, we present the seismic data, method and procedure, the inferred apparent splitting parameters, the splitting parameters associated with the anisotropy in the shallow mantle beneath seismic stations and the anisotropy at the base of the African Anomaly, and the implications of the inferred anisotropy in the lowermost mantle.

2. Seismic Observation, Method and Procedure

2.1. Seismic Observation

[5] We collect about 1600 SKS and SKKS waveforms of deep earthquakes recorded at distances from 90° to 150° by the seismic stations in three temporary PASSCAL broadband seismic arrays: the Kaapvaal seismic array (1997–1999), the Tanzania seismic array (1994–1995), and the Ethiopia/Kenya seismic array (1999–2001), as well as the permanent stations in the Global Seismographic Network (GSN) deployed in Africa and Europe. The SKKS waveforms are processed with the Hilbert transformation to be consistent with the SKS waveforms for the same earthquake. A frequency bandpass filter of 0.02–0.5 Hz is applied to all seismic data. From the 1600 waveforms, we choose 415 SKS and 111 SKKS waveforms of 127 deep earthquakes (Table S1 in the auxiliary material[1]) on the basis of waveform quality, and obtain a total of 526 pairs of reliable measurements for apparent splitting parameters (Table S2). These high-quality seismic data provide good coverage for some portion of the VLVP and the surrounding areas (Figure 1a).

2.2. Method and Procedure

[6] Because of the P to S conversion at the CMB, the splitting of SKS and SKKS waveforms is affected by the anisotropy only along their propagation paths in the receiver-

[1] Auxiliary material data sets are available at ftp://ftp.agu.org/apend/jb/2006jb004719.

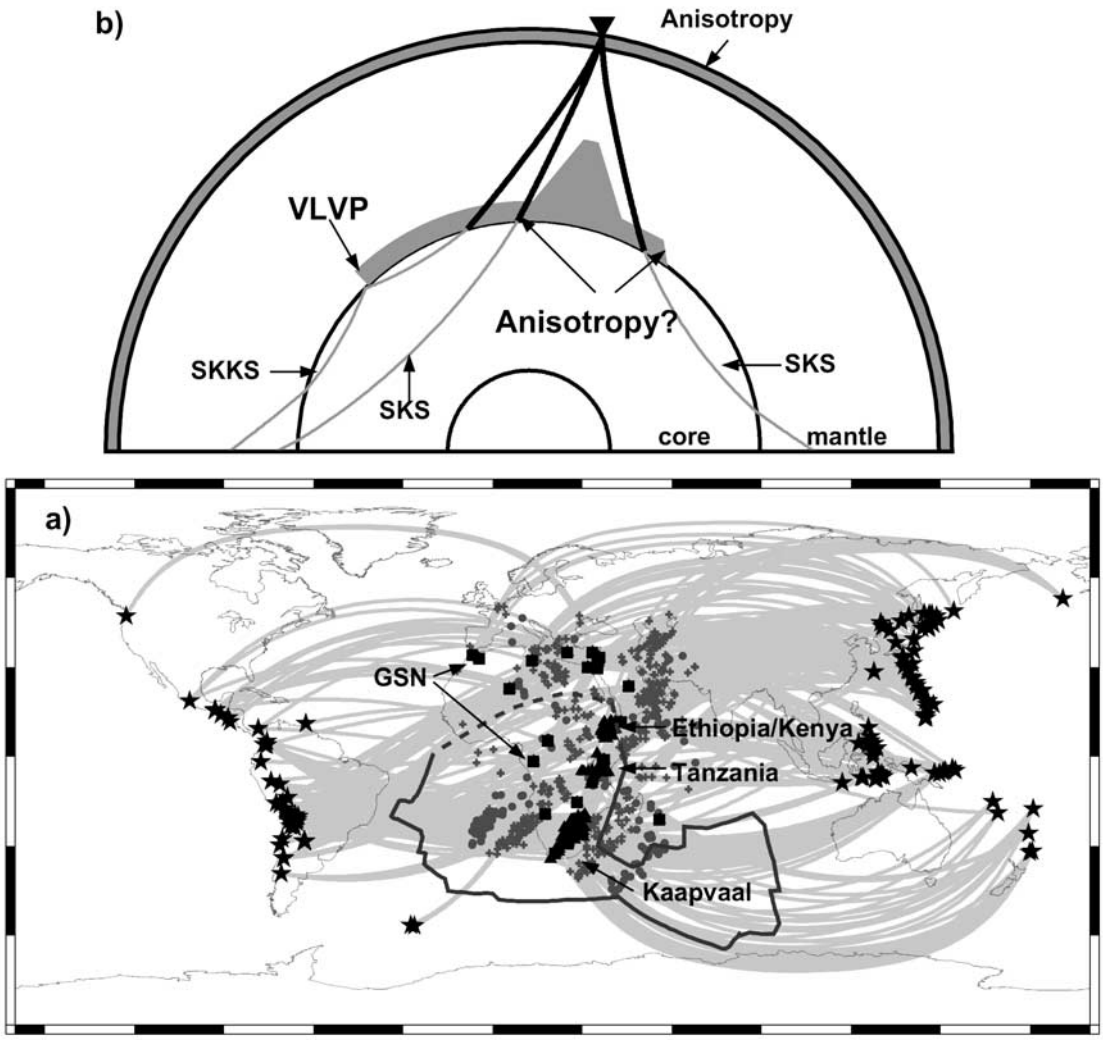

Figure 1. (a) Map view of great circle paths (gray traces), locations of SKS (gray crosses) and SKKS (gray dots) exit points at the CMB, earthquakes (black stars) and seismic stations (black triangles and squares) in the Kaapvaal seismic array (1997–1999), the Tanzania seismic array (1994–1995), the Ethiopia/Kenya seismic array (1999–2001), and the GSN. The black contour represents the geographic boundary of the VLVP [*Wang and Wen*, 2004] with the dashed portion less constrained due to the nature of the seismic data. (b) Raypaths (gray traces) of SKS and SKKS phases. The splitting of the SKS and SKKS waveforms is sensitive to the anisotropy only along the propagation paths in the receiver-side mantle, highlighted in black. The gray basal layer above the CMB represents the VLVP, and the gray layer at the top of the mantle represents an anisotropic layer in the shallow mantle.

side mantle (the highlighted portion in Figure 1b). In the study, we simplify our anisotropy model by assuming that anisotropy exists only in the shallow mantle and in the lowermost mantle, and the rest of the mantle is isotropic (Figure 1b). That is, our anisotropy model has two single anisotropic layers with the first layer in the lowermost mantle near SKS and SKKS exit points at the CMB and the second layer in the shallow mantle beneath seismic stations (Figure 1b). The medium is further assumed to possess hexagonal symmetry with a horizontal symmetry axis in each anisotropic layer, and SKS and SKKS waves are split once every time they propagate through an anisotropic layer [*Yardley and Crampin*, 1991].

[7] Our goal is to study the seismic anisotropy near the SKS and SKKS exit points at the CMB. We adopt a three-step approach. We first measure apparent splitting parameters (fast polarization direction and delay time) by minimizing energy on the tangential component of SKS or SKKS waveforms [*Silver and Chan*, 1991]. These apparent splitting parameters should be interpreted in the presence of two anisotropic layers. We then determine the anisotropy in the shallow mantle beneath seismic stations by searching the common apparent splitting parameters for SKS and SKKS phases that can be reasonably attributed to the shallow mantle anisotropy. Consistency of measurements for SKS and SKKS waveforms originated from the same earth-

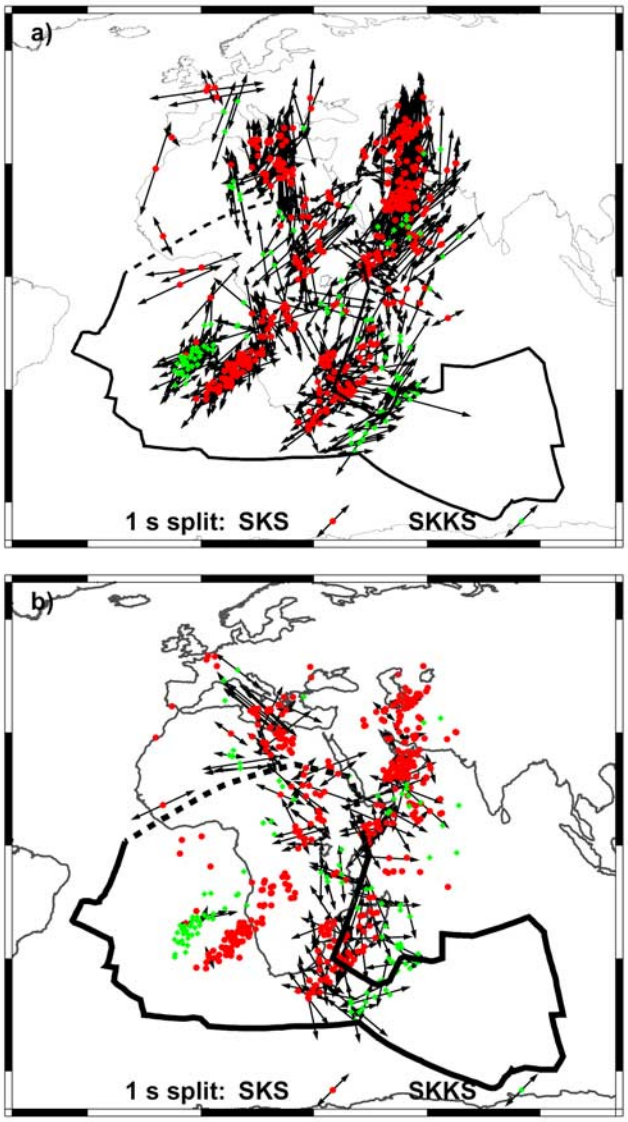

Figure 2. (a) Apparent splitting parameters (black arrows) obtained using SKS and SKKS waveforms and plotted at the SKS (red dots) and SKKS (green squares) exit points at the CMB, with the directions of the arrows pointing to fast polarization directions and the lengths of the arrows scaled to delay times. The black contour represents the geographic boundary of the VLVP. (b) Similar to Figure 2a, but for the splitting parameters for the lowermost mantle anisotropy measured using the SKS and SKKS waveforms corrected for the shallow mantle anisotropy beneath seismic stations.

quakes is used to weight observations that contribute to the shallow mantle anisotropy estimation. Also, the common variations in the apparent splitting parameters with seismic stations, but not with the CMB exit points, require that the major cause to be at shallow depths beneath seismic stations. This turns out to exclude the seismic data that sample near the VLVP margins. After the anisotropy in the shallow mantle is determined from the SKS and SKKS data that sample the regions away from the VLVP margins, we remove influence of the inferred shallow mantle anisotropy beneath seismic stations on the SKS and SKKS waveforms, and obtain the splitting parameters related to the anisotropy near SKS and SKKS exit points at the CMB.

3. Seismic Results

3.1. Apparent Splitting Parameters

[8] We obtain 526 pairs of reliable measurements for apparent splitting parameters using 415 from SKS and 111 from SKKS waveforms (Figure 2a). The apparent splitting parameters (fast polarization direction and delay time) are measured by minimizing energy on the tangential component of SKS or SKKS waveforms, following the procedures outlined by *Silver and Chan* [1991]. The apparent splitting parameters exhibit different characteristics for the seismic data sampling the border of the VLVP and those sampling the regions far away from the VLVP border.

[9] When SKS and SKKS waves sample the areas far away from the VLVP border, the apparent splitting parameters obtained using SKS waveforms are consistent with those obtained using SKKS waveforms from the same earthquake. Take the SKS and SKKS phases of event 1997/09/02 whose exit points at the CMB are in the interior of the VLVP for example (event 1 in Figure 3). Both SKS and SKKS show clear energy on the tangential component, diagnostic of shear wave splitting (see examples in Figures S1a and S1b). The apparent fast polarization directions obtained from both SKS and SKKS waves are consistent with each other. They change gradually from 11°N to 80°N across the seismic array from south to north, and rotate back to the North direction over short distances for the northernmost stations. The measured delay times obtained from SKS and SKKS waves are also similar. For

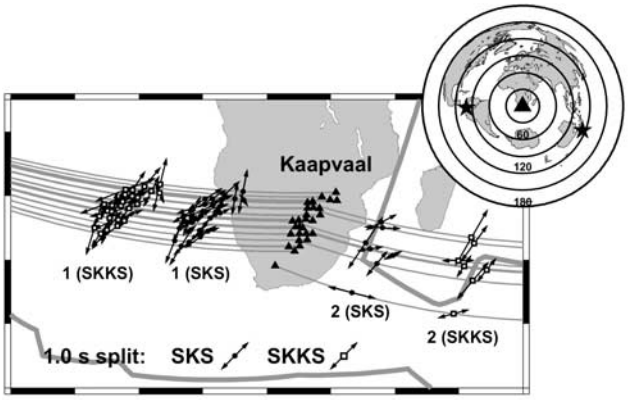

Figure 3. Apparent splitting parameters (black arrows) obtained using SKS and SKKS waveforms of events 1997/09/02 (labeled as 1) and 1997/12/22 (labeled as 2), recorded by seismic stations in the Kaapvaal seismic array (black triangles). These measurements are plotted at the SKS (black solid dots) and SKKS (black open squares) exit points at the CMB, with the arrows pointing to fast polarization directions and the lengths of the arrows scaled to delay times. The gray traces show the great circle paths from earthquakes to stations. The heavy gray contour represents the geographic boundary of the VLVP. Locations of the two earthquakes (black stars) and the Kaapvaal seismic array (black triangle) are shown on the top right insert.

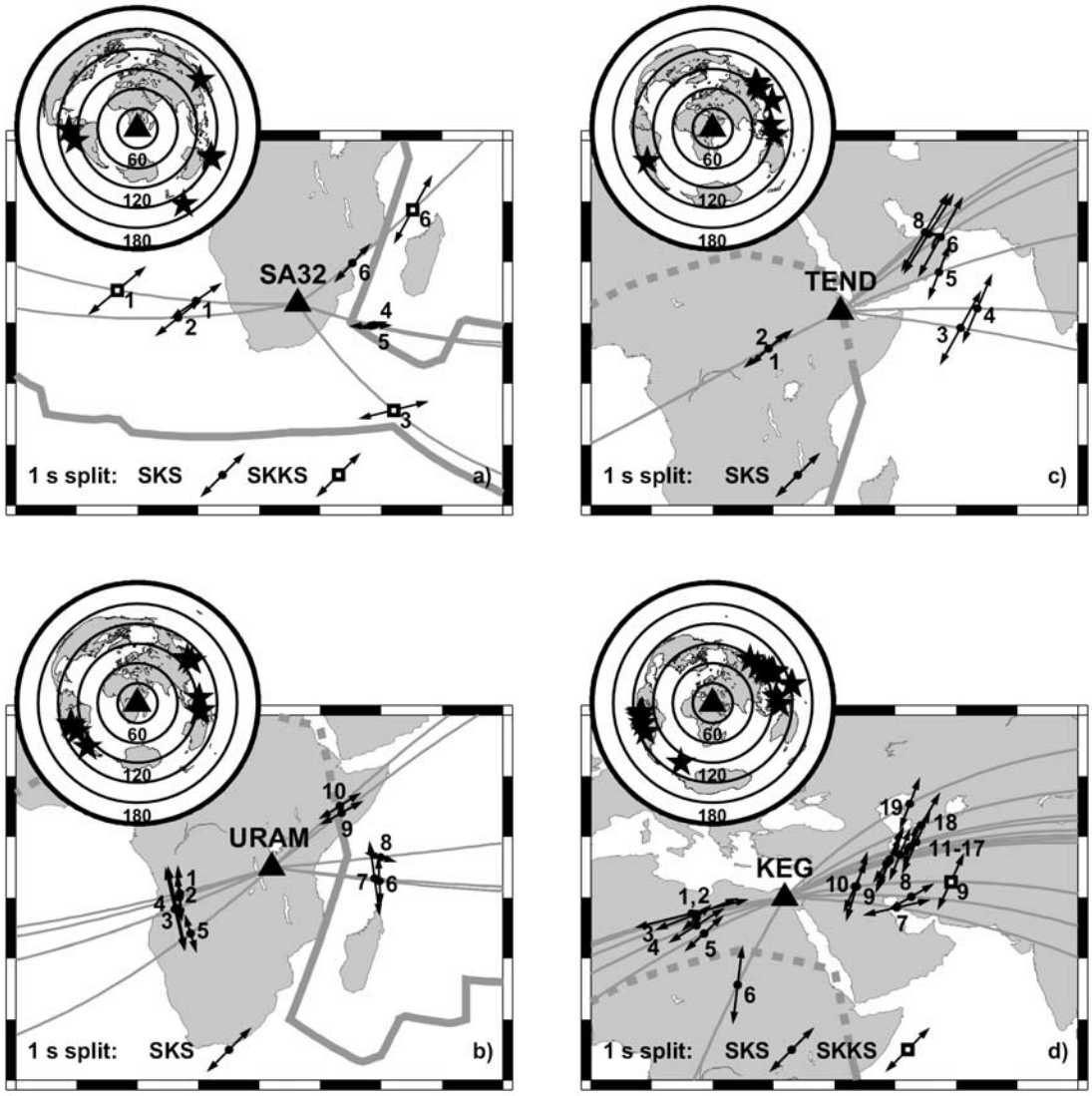

Figure 4. Apparent splitting parameters (black arrows) obtained using SKS and SKKS waveforms recorded by stations (a) SA32, (b) URAM, (c) TEND, and (d) KEG. These measurements are plotted at the SKS (black solid dots) and SKKS (black open squares) exit points at the CMB, and labeled as event numbers, with the arrows pointing to the fast polarization directions and the lengths of the arrows scaled to delay times. The gray traces are the great circle paths from earthquakes to the recording station (black triangle). The heavy gray contour represents the geographic boundary of the VLVP. Locations of earthquakes (black stars) and the recording station (black triangle) are shown on the top left inserts.

all our collected SKS and SKKS waveforms originated from the same earthquakes, we observe small difference (the average is about $7^\circ \pm 5^\circ$) in apparent fast polarization direction for the seismic data sampling the regions away from the border of the VLVP.

[10] The apparent splitting parameters obtained from the analyses of those SKS and SKKS waveforms also show a strong correlation with seismic station and weak dependence on the SKS and SKKS back azimuth. Here, we present several examples of apparent splitting parameters for the seismic data recorded by stations SA32, a station in the Kaapvaal seismic array, URAM, a station in the Tanzania seismic array, TEND, a station in the Ethiopia/Kenya seismic array, and KEG, a station of the GSN (Figure 4). For station SA32, the SKS and SKKS of event 1997/09/02 (event 1 in Figure 4a) and the SKS of event 1998/04/03 (event 2 in Figure 4a) sample the interior of the VLVP and their apparent splitting parameters are similar with a fast polarization direction of about 52°N and a delay time of about 1.1 s (Figure 4a). For station URAM, the SKS waves of events 1–5 also sample the interior of the VLVP. Despite some scatter in the measured delay times, most measured fast polarization directions point to −5°N (Figure 4b). Similar features are also observed for the apparent splitting parameters obtained using SKS and SKKS waves sampling outside the VLVP. For example, for station TEND, the analysis of the SKS waveforms of events 3–8 yields similar apparent splitting parameters, with a fast polarization direc-

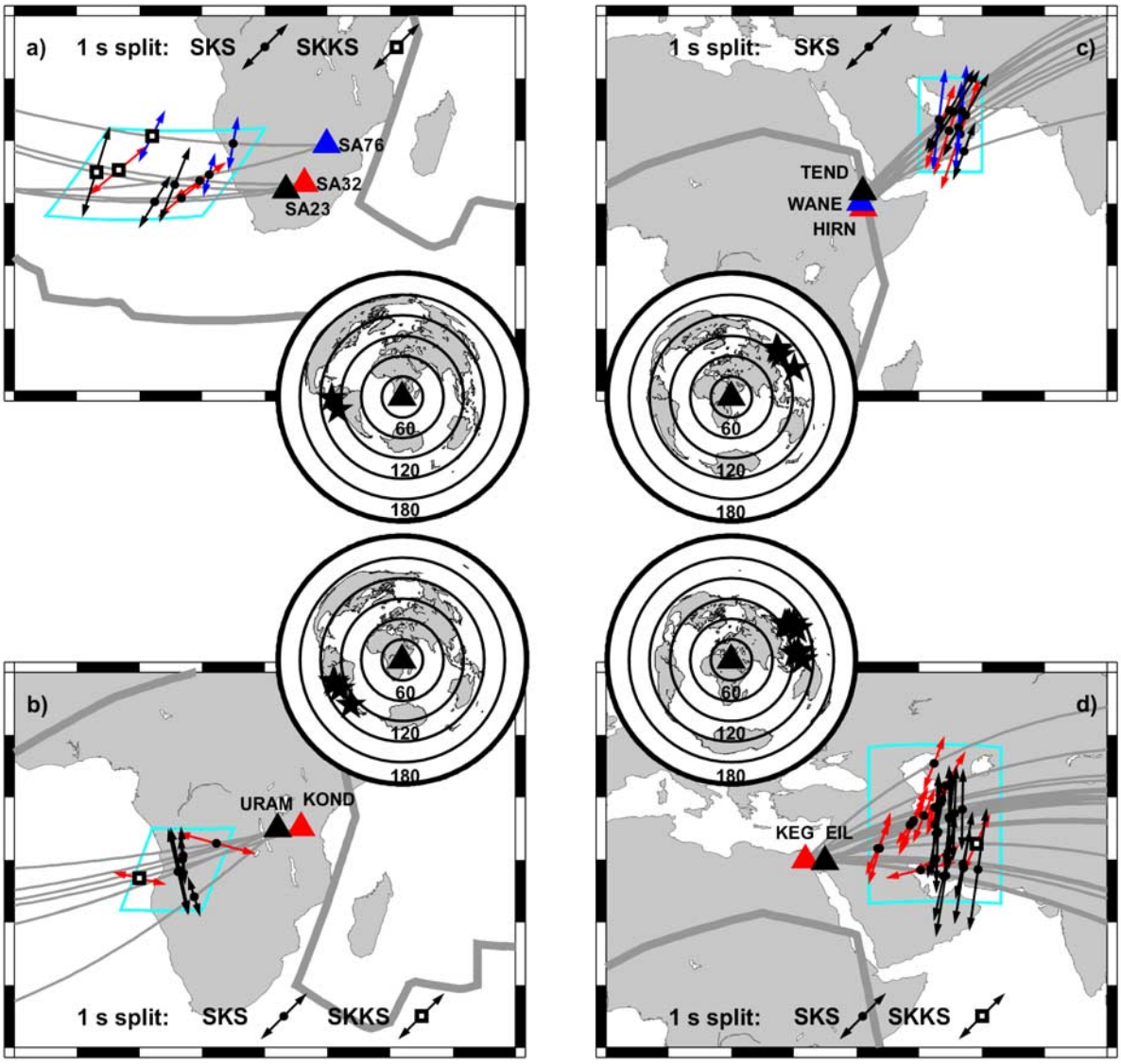

Figure 5. Apparent splitting parameters (arrows) obtained using SKS and SKKS waveforms recorded by some stations in (a) the Kaapvaal seismic array, (b) the Tanzania seismic array, (c) the Ethiopia/Kenya seismic array, and (d) the GSN. These arrows are color coded by the recording seismic station and plotted at the SKS (black solid dots) and SKKS (black open squares) exit points at the CMB, with the arrows pointing to the fast polarization directions and the lengths of the arrows scaled to delay times. The exit points at the CMB for the SKS and SKKS phases are within a small area enclosed by the light blue frame. The gray contour represents the geographic boundary of the VLVP. Locations of these earthquakes (black stars) and stations (triangles) are shown on the inserts in the center.

tion of 29°N and a delay time of 1.5 s (Figure 4c). For station KEG, the analysis of the observations for SKS and SKKS of events 9–19 yields almost identical apparent splitting parameters, with a fast polarization direction of 23°N and a delay time of 1.15 s (Figure 4d).

[11] Furthermore, the apparent splitting parameters obtained from the seismic data sampling away from the VLVP margins do not correlate with the exit points of these seismic phases at the CMB. They show variations for the seismic data sampling a similar area at the CMB (Figure 5), indicating that for those seismic data, the apparent splitting parameters cannot be explained by the anisotropy in the lowermost mantle near the exit points of the SKS and SKKS phases at the CMB.

[12] However, when SKS and SKKS waves sample near the border of the VLVP, we observe different apparent splitting parameters obtained using SKS and SKKS waves originated from the same earthquake. For example, both SKS and SKKS phases of event 1997/12/22 (event 2 in Figure 3) sample the border of the VLVP and apparent splitting parameters obtained from the SKS wave analyses show different fast polarization directions from those from the SKKS wave analyses. These apparent splitting parameters also differ from those obtained from the SKS and

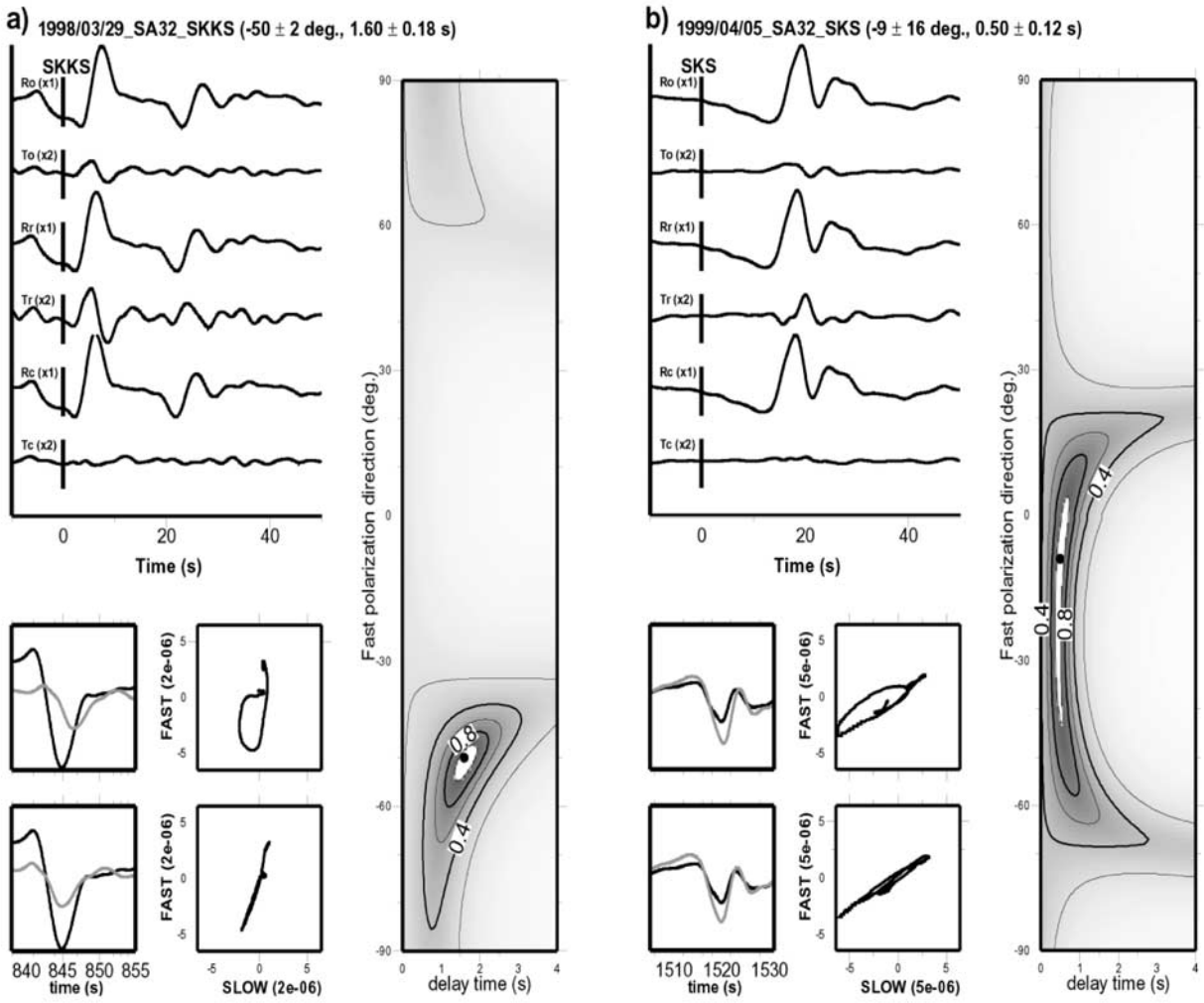

Figure 6. Examples of waveform splitting analyses of the lowermost mantle anisotropy for (a) SKKS of event 1998/03/29 (event 3 in Figure 4a) and (b) SKS of event 1999/04/05 (event 5 in Figure 4a) recorded by station SA32. Figures 6a and 6b are labeled by event date_station_phase (fast polarization direction ±1 sigma error in degree, delay time ±1 sigma error in second). (top left) For each example, the original radial (Ro) and tangential (To) displacements, the radial (Rr) and tangential (Tr) displacements of SKS or SKKS waves after corrected for the shallow mantle anisotropy beneath seismic station (52°N, 1.10 s), the unsplit radial (Rc) and tangential (Tc) displacements of SKS or SKKS waves after further corrected for the anisotropy in the lowermost mantle. The vertical black lines show the predicted arrival time of SKS or SKKS based on model IASP 91 [*Kennett and Engdahl*, 1991]. (bottom left) Superposition of fast (black) and slow (gray) components, (middle left) uncorrected and (bottom left) corrected, and their corresponding horizontal particle motions (in millimeter), (middle right) uncorrected and (bottom right) corrected. (right) Contour plot of normalized energy on the corrected transverse component as a function of fast polarization direction and delay time. The solid black dot indicates the optimum fast polarization direction and delay time that minimize energy on the tangential component of SKS or SKKS waveforms, and the white area represents best fitting parameters at the 95% confidence level. The energy is normalized to that of the best fitting fast polarization direction and delay time at the 95% confidence level.

SKKS waveforms of event 1997/09/02 (event 1 in Figure 3) whose exit points at the CMB are in the interior of the VLVP. For all our available SKS and SKKS waveforms originated from the same earthquakes, we observe much larger difference (the average is about 39° ± 10°) in the apparent fast polarization directions for the seismic data sampling the border of the VLVP than those for the seismic data sampling away from the border of the VLVP.

[13] The inferred fast polarization directions, obtained from the SKS and SKKS waves sampling the border of the VLVP, no longer correlate with seismic station and they vary over small distance and with the back azimuth of the SKS and SKKS phases. For example, for station SA32, the

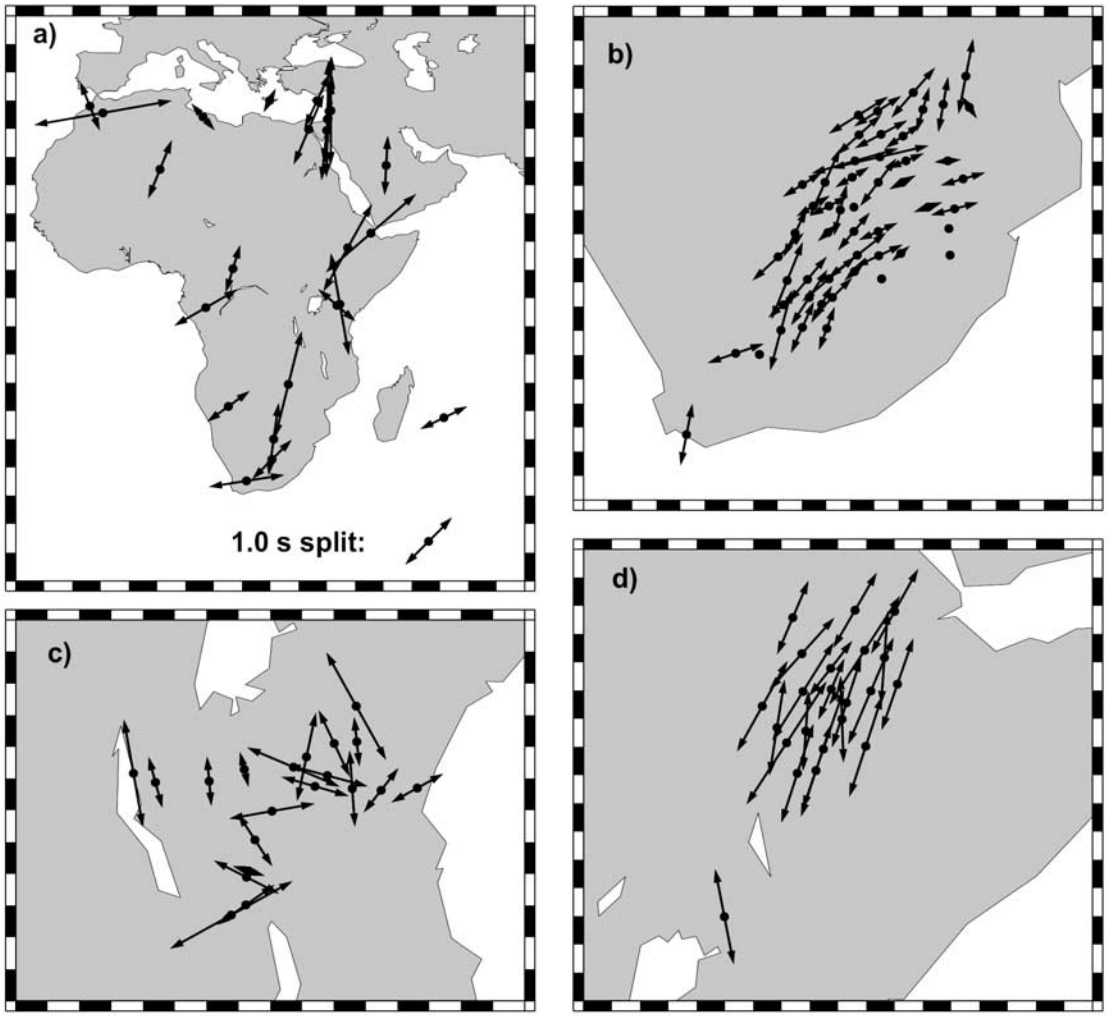

Figure 7. Splitting parameters (black arrows) inferred for the anisotropy in the shallow mantle beneath the seismic stations in (a) the GSN, (b) the Kaapvaal seismic array, (c) the Tanzania seismic array, and (d) the Ethiopia/Kenya seismic array. These measurements are plotted at the locations of seismic station (black solid dots). The splitting parameters for the shallow mantle anisotropy are obtained using the waveforms of the SKS and SKKS phases sampling the regions far away from the VLVP border (inside or outside the VLVP). The arrows point to the fast polarization directions and the lengths of the arrows are scaled to delay times. The dots without an arrow indicate null observations in the shear wave splitting analyses.

SKKS of event 1998/03/29 (event 3 in Figure 4a) and the SKS of event 1999/04/05 (event 4 in Figure 4a) sample the border of the VLVP. The measured apparent splitting parameters are different from each other and from those obtained from the analysis of the SKS and SKKS of events 1 and 2 that sample the interior of the VLVP (Figures 4a, 6, and S2). For station URAM, the SKS phases of events 8, 9 and 10 sample the border of the VLVP, and the apparent splitting parameters for them are different from those for SKS of events 1 to 7 that do not sample near the border (Figure 4b). For station TEND, the apparent splitting parameters obtained using the SKS of events 1 and 2 are different from those for the SKS of events 3–8 sampling outside the VLVP (Figure 4c). For station KEG, the apparent splitting parameters for events 1–6 are also different from those for SKS and SKKS of events 9–19 sampling outside the VLVP away from the border (Figures 4d and S3).

3.2. Anisotropy in the Shallow Mantle Beneath Seismic Stations

[14] For the apparent splitting parameters obtained from the seismic data sampling away from the VLVP margins, because they are consistent with each other between those obtained using SKS and SKKS phases from the same earthquake and their variations strongly correlate with seismic stations but not with the SKS and SKKS exit points at the CMB, we attribute them to the anisotropy in the shallow mantle beneath seismic stations. Our rationale is as follows. If anisotropy in the lowermost mantle does not contribute to waveform splitting, the apparent splitting parameters obtained from the SKS waveforms would be

the same as those obtained from the SKKS waveforms recorded for the same earthquake because SKS and SKKS waves have almost identical propagation paths in the shallow mantle. In this case, the apparent splitting parameters would also strongly correlate with seismic station. On the other hand, those common apparent splitting parameters cannot be explained by anisotropy in the lowermost mantle because the observations for SKS and SKKS waves recorded by various seismic stations, but sample a similar area at the CMB, show varying apparent splitting parameters between stations (Figure 5). In other words, when the anisotropy in the shallow mantle provides a reasonable explanation to the apparent splitting parameters while the lowermost mantle anisotropy does not, we attribute them to the shallow mantle anisotropy. The weak dependence on the sampling azimuth of the apparent splitting parameters for the data sampling away from the VLVP margins further supports our assumption of a single layer of anisotropy in the shallow mantle beneath seismic stations, as the weak azimuthal dependence is inconsistent with two shallow strongly anisotropic layers beneath seismic stations (for example, the lithosphere and the underlying asthenosphere) [*Silver and Savage*, 1994; *Hartog and Schwartz*, 2001].

[15] We obtain the splitting parameters related to the anisotropy in the shallow mantle by averaging the apparent splitting parameters obtained from the seismic data sampling areas away from the border of the VLVP (Figure 7; see Table S3). Our obtained shallow mantle anisotropy beneath seismic stations generally agrees with previous results [*Barruol and Ismail*, 2001; *Silver et al.*, 2001; *Walker et al.*, 2004; *Gashawbeza et al.*, 2004], although the seismic data sampling the VLVP margins were included in the analyses of shallow anisotropy in those previous studies. This is due to the fact that the SKS and SKKS phases sampling the VLVP margins constitute a small portion of the data set.

3.3. Lowermost Mantle Anisotropy Associated With the VLVP

[16] After the splitting parameters for the shallow anisotropy are obtained, we remove the influence of the shallow anisotropy on the seismic waveforms and obtain the splitting parameters related to the lowermost mantle anisotropy on the basis of the splitting analysis of the corrected waveforms. The removal of the influence of the shallow mantle anisotropy is carried out by projecting the radial and tangential components of the SKS and SKKS phases onto the fast and slow axes of the shallow mantle anisotropy, advancing the slow component by the delay time and projecting the fast and slow components back onto the radial and tangential axes. We measure the splitting parameters related to the lowermost mantle anisotropy by minimizing energy on the tangential component of the corrected waveforms. Two examples are shown in Figure 6 for the SKKS of event 1998/03/29 (event 3 in Figure 4a) and the SKS of event 1999/04/05 (event 4 in Figure 4a) recorded by station SA32. While the inferred splitting parameters for the lowermost mantle anisotropy show, as expected, absence of shear wave splitting (dots and squares in Figure 2b) in the regions away from the border of the VLVP, they reveal a complex pattern with delay times of about 1.0 s and fast polarization directions changing over small distances near the border of the VLVP (Figure 2b).

4. Discussions

[17] The inferred complex anisotropy near the border of the VLVP may be generated by the LPO of intrinsically anisotropic mineral aggregates in the lowermost mantle. Because of the shearing between the surrounding normal mantle and the VLVP, strain accumulation near the border of the VLVP may orient a particular axis of the intrinsically anisotropic mineral aggregates to the local maximal shearing directions, causing azimuthal anisotropy near the border of the VLVP. The inferred complex anisotropy pattern suggests that the flow pattern is complex in the margin of the VLVP.

[18] A similar complex pattern of seismic anisotropy was also reported near the border of another large-scale low-velocity province near the core-mantle boundary beneath Pacific, the "Pacific Anomaly" [*Russell et al.*, 1998, 1999; *Ford et al.*, 2006], which also likely represents a chemical anomaly [e.g., *To et al.*, 2005; *He et al.*, 2006]. At the same time, *Thorne et al.* [2004] and *Wen* [2006] reported that many hot spots (for example, Reunion, Comoros, Bouvet and Shona) were geographically adjacent to the VLVPs. The reported complex anisotropy in this study may further indicate that the interactions of the VLVPs with their surrounding mantle are strong and generate complex mantle flow that gives rise to favorable conditions (such as local thickening of the bottom thermal boundary layer) for development of mantle thermal plumes near their margins. Such scenario is also consistent with the presence of strong small-scale heterogeneities at the core-mantle boundary near the VLVP margins [e.g., *Wen*, 2000]. The complex seismic anisotropy associated with the VLVPs would be useful for placing constraints on the dynamics of the deep mantle by coupling with geodynamic modeling [e.g., *McNamara and Zhong*, 2005; *Zhong*, 2006].

5. Conclusions

[19] We constrain the anisotropy associated with a VLVP beneath the South Atlantic and Indian Oceans at the base of the Earth's mantle, using the splitting of SKS and SKKS waves sampling the region. We first infer the anisotropy in the shallow mantle by examining the consistency between the apparent splitting parameters inferred from the SKS phases and those inferred from the SKKS phases, the correlation of the apparent splitting parameters with seismic station and the exit points of the seismic phases at the CMB, and the azimuthal dependence of the apparent splitting parameters. Those analyses suggest that the apparent splitting parameters inferred from the seismic data sampling the regions away from the VLVP margins can be attributed to anisotropy in the shallow depths beneath the seismic stations, but not to anisotropy in the lowermost mantle. Those apparent splitting parameters are thus used to infer the shallow anisotropy beneath the seismic stations. We obtain the splitting parameters associated with the seismic anisotropy in the lowermost mantle on the basis of the seismic data corrected for the influence of the shallow anisotropy beneath the seismic stations. Our results reveal a complex

pattern of anisotropy near the border of the VLVP, with splitting delay times of about 1.0 s and fast polarization directions changing over small distances. Such a complex anisotropy pattern may be explained by lattice-preferred orientation of anisotropic mantle aggregates aligned by a complex mantle flow near the VLVP margins. The complex flow pattern near the VLVP margins indicates strong interactions of the VLVP, a compositional anomaly, with the surrounding mantle, and may provide an explanation to the concentration of some hot spots geographically near the borders of the VLVPs in the lowermost mantle.

[20] **Acknowledgments.** We are grateful to the Incorporated Research Institution for Seismology for supplying data. The seismic data used were collected from the GSN, Kaapvaal, Tanzania, and Ethiopia/Kenya seismic arrays. We thank the principal academic collaborators and investigators of all four arrays for their efforts in collecting the seismic data and Andy Nyblade for generously making the Ethiopia/Kenya data available to us before they were released. We also thank Thorne Lay, Edward Garnero, and the Associate Editor Michael Ritzwoller for helpful comments that have significantly improved the presentation of this paper. This project was supported by NFS grants EAR-0309859 and EAR-0609717.

References

Barruol, G., and W. B. Ismail (2001), Upper mantle anisotropy beneath the African IRIS and Geoscope stations, *Geophys. J. Int.*, *145*, 549–561.

Dziewonski, A., and D. L. Anderson (1981), Preliminary reference Earth model, *Phys. Earth Planet. Inter.*, *25*, 297–356.

Ford, S. R., E. J. Garnero, and A. K. McNamara (2006), A strong lateral shear velocity gradient and anisotropy heterogeneity in the lowermost mantle beneath the southern Pacific, *J. Geophys. Res.*, *111*, B03306, doi:10.1029/2004JB003574.

Fouch, M. J., K. M. Fischer, and M. E. Wysession (2001), Lowermost mantle anisotropy beneath the Pacific: Imaging the source of the Hawaiian plume, *Earth Planet. Sci. Lett.*, *190*, 167–180.

Garnero, E. J., and T. Lay (1997), Lateral variations in lowermost mantle shear wave anisotropy, *J. Geophys. Res.*, *102*, 8121–8135.

Garnero, E. J., and T. Lay (2003), D″ Shear velocity heterogeneity, anisotropy and discontinuity structure beneath the Caribbean and Central America, *Phys. Earth Planet. Inter.*, *140*, 219–242.

Garnero, E. J., M. M. Moore, T. Lay, and M. J. Fouch (2004), Isotropy or weak vertical transverse isotropy in D″ beneath the Atlantic Ocean, *J. Geophys. Res.*, *109*, B08308, doi:10.1029/2004JB003004.

Gashawbeza, E. M., S. L. Klemperer, A. A. Nyblade, K. T. Walker, and K. M. Keranen (2004), Shear-wave splitting in Ethiopia: Precambrian mantle anisotropy locally modified by Neogene rifting, *Geophys. Res. Lett.*, *31*, L18602, doi:10.1029/2004GL020471.

Grand, S. P., R. D. van der Hilst, and S. Widiyantoro (1997), Global seismic tomography: A snapshot of convection in the Earth, *GSA Today*, *7*, 1–7.

Gurnis, M., J. X. Mitrovica, J. Ritsema, and H. van Heijst (2000), Constraining mantle density structure using geological evidence of surface uplift rates: The case of the African Superplume, *Geochem. Geophys. Geosyst.*, *1*(7), doi:10.1029/1999GC000035.

Hartog, R., and S. Y. Schwartz (2001), Depth-dependent mantle anisotropy below the San Andreas fault system: Apparent splitting parameters and waveforms, *J. Geophys. Res.*, *106*, 4155–4167.

He, Y., L. Wen, and T. Zheng (2006), Geographic boundary and shear velocity structure of the "Pacific anomaly" near the core-mantle boundary beneath western Pacific, *Earth Planet. Sci. Lett.*, *244*, 302–314.

Ishii, M., and J. Tromp (1999), Normal-mode and free-air gravity constraints on lateral variations in velocity and density of the Earth's mantle, *Science*, *285*, 1231–1236.

Karato, S. I. (1998), Seismic anisotropy in the deep mantle, boundary layers and the geometry of mantle convection, *Pure Appl. Geophys.*, *151*, 565–587.

Kendall, J. M. (2000), Seismic anisotropy in the boundary layers of the mantle, in *Earth's Deep Interior: Mineral Physics and Tomography From the Atomic to the Global Scale*, *Geophys. Monogr. Ser.*, vol. 117, edited by S. Karato et al., pp. 63–87, AGU, Washington, D. C., pp. 133–159.

Kendall, J. M., and P. G. Silver (1996), Constraints from seismic anisotropy on the nature of the lowermost mantle, *Nature*, *381*, 409–412.

Kendall, J. M., and P. G. Silver (1998), Investigating causes of D″ anisotropy, *The Core-Mantle Boundary Region*, *Geodyn. Ser.*, vol. 28, edited by M. Gurnis et al., pp. 97–118, AGU, Washington, D. C.

Kennett, B. L. K., and E. R. Engdahl (1991), Travel times for global earthquake location and phase identification, *Geophys. J. Int.*, *122*, 429–465.

Lay, T., Q. Williams, and J. Garnero (1998), The core-mantle boundary layer and deep Earth dynamics, *Nature*, *392*, 461–468.

Li, X. D., and B. Romanowicz (1996), Global mantle shear velocity model developed using nolinear asymptotic coupling theory, *J. Geophys. Res.*, *101*, 22,245–22,273.

Lithgow-Bertelloni, C., and P. G. Silver (1998), Dynamic topography, plate driving forces and the African superswell, *Nature*, *395*, 269–272.

Masters, G., S. Johnson, G. Laske, and H. Bolton (1996), A shear velocity model of the mantle, *Philos. Trans. R. Soc. London*, *354*, 1385–1411.

Masters, G., G. Laske, H. Bolton, and A. Dziewonski (2000), Earth's Deep interior: Mineral physics and tomography from the atomic to the global scale, in *Earth's Deep Interior: Mineral Physics and Tomography From the Atomic to the Global Scale*, *Geophys. Monogr. Ser.*, vol. 117, edited by S. Karato et al., pp. 63–87, AGU, Washington, D. C.

Matzel, E., M. K. Sen, and S. P. Grand (1996), Evidence for anisotropy in the deep mantle beneath Alaska, *Geophys. Res. Lett.*, *23*, 2417–2420.

Maupin, V., E. J. Garnero, T. Lay, and M. J. Fouch (2005), Azimuthal anisotropy in the D″ layer beneath the Caribbean, *J. Geophys. Res.*, *110*, B08301, doi:10.1029/2004JB003506.

McNamara, A. K., and S. J. Zhong (2005), Thermochemical structures beneath Africa and the Pacific Ocean, *Nature*, *437*, 1136–1139.

Ni, S., and D. V. Helmberger (2003a), Ridge-like lower mantle structure beneath South Africa, *J. Geophys. Res.*, *108*(B2), 2094, doi:10.1029/2001JB001545.

Ni, S., and D. V. Helmberger (2003b), Seismological constraints on the South African superplume: Could be the oldest distinct structure on earth, *Earth Planet. Sci. Lett.*, *206*, 119–131.

Ni, S., and D. V. Helmberger (2003c), Further constraints on the African superplume structure, *Phys. Earth Planet. Inter.*, *140*, 243–251.

Ni, S., E. Tan, M. Gurnis, and D. V. Helmberger (2002), Sharp sides to the African super plume, *Science*, *296*, 1850–1852.

Niu, F., and A. M. Perez (2004), Seismic anisotropy in the lower mantle: A comparison of waveform splitting of SKS and SKKS, *Geophys. Res. Lett.*, *31*, L24612, doi:10.1029/2004GL021196.

Panning, M., and B. Romanowicz (2004), Inference on flow at the base of Earth's mantle based on seismic anisotropy, *Science*, *303*, 351–353.

Pulliam, J., and M. K. Sen (1998), Seismic anisotropy in the core-mantle transition zone, *Geophys. J. Int.*, *135*, 113–128.

Restivo, A., and G. Helffrich (2006), Core-mantle boundary structure investigated using SKS and SKKS polarization anomalies, *Geophys. J. Int.*, *165*, 288–302.

Ritsema, J. (2000), Shear velocity anisotropy in the lowermost mantle beneath the Indian Ocean, *Geophys. Res. Lett.*, *27*, 1041–1044.

Ritsema, J., T. Lay, E. J. Garnero, and H. Benz (1998), Seismic anisotropy in the lowermost mantle beneath the Pacific, *Geophys. Res. Lett.*, *25*, 1229–1232.

Ritsema, J., H. J. van Heijst, and J. H. Woodhouse (1999), Complex shear wave velocity structure imaged beneath Africa and Iceland, *Science*, *286*, 1925–1928.

Rokosky, J. M., T. Lay, E. J. Garnero, and S. A. Russell (2004), High-resolution investigation of shear wave anisotropy in D″ beneath the Cocos Plate, *Geophys. Res. Lett.*, *31*, L07605, doi:10.1029/2003GL018902.

Rokosky, J. M., T. Lay, and E. Garnero (2006), Small-scale lateral variations in azimuthally anisotropic D″ structure beneath the Cocos Plate, *Earth Planet. Sci. Lett.*, *248*, 411–425.

Russell, S. A., T. Lay, and E. J. Garnero (1998), Seismic evidence for small-scale dynamics in the lowermost mantle at the root of the Hawaiian hotspot, *Nature*, *396*, 255–258.

Russell, S. A., T. Lay, and E. J. Garnero (1999), Small scale lateral shear velocity and anisotropy heterogeneity near the core-mantle boundary beneath the central Pacific imaged using broadband ScS waves, *J. Geophys. Res.*, *104*, 13,183–13,199.

Silver, P. G., and W. W. Chan (1991), Shear-wave splitting and subcontinental mantle deformation, *J. Geophys. Res.*, *96*, 16,429–16,454.

Silver, P. G., and W. Holt (2002), The mantle flow field beneath western North America, *Science*, *295*, 1054–1057.

Silver, P. G., and M. Savage (1994), The interpretation of shear-wave splitting parameters in the presence of two anisotropic layers, *Geophys. J. Int.*, *119*, 949–963.

Silver, P. G., S. S. Gao, K. H. Liu, and the Kaapvaal Seismic Group (2001), Mantle deformation beneath southern Africa, *Geophys. Res. Lett.*, *28*, 2493–2496.

Su, W. J., R. L. Woodward, and A. M. Dziewonski (1994), Degree 12 model of shear velocity heterogeneity in the mantle, *J. Geophys. Res.*, *99*, 6945–6980.

Thomas, C., and J. M. Kendall (2002), The lowermost mantle beneath northern Asia: 2. Evidence for lower-mantle anisotropy, *Geophys. J. Int.*, *151*, 296–308.

Thorne, M., E. J. Garnero, and S. Grand (2004), Geographic correlation between hot spots and deep mantle lateral shear-wave velocity gradients, *Phys. Earth Planet. Inter.*, *146*, 47–63.

To, A., B. Romanowicz, Y. Capdeville, and N. Takeuchi (2005), 3D effects of sharp boundaries at the borders of the African and Pacific Superplumes: Observation and modeling, *Earth Planet. Sci. Lett.*, *233*, 137–153.

Trampert, J., F. Deschamps, J. Resovsky, and D. Yuen (2004), Probabilistic tomography maps chemical heterogeneities throughout the lower mantle, *Science*, *306*, 853–856.

van der Hilst, R. D., S. Widyantoro, and E. R. Engdahl (1997), Evidence for deep mantle circulation from global tomography, *Nature*, *386*, 578–584.

Vinnik, L., B. Romanowicz, Y. L. Stunff, and L. Makeyeva (1995), Seismic anisotropy in the D″ layer, *Geophys. Res. Lett.*, *22*, 1657–1660.

Vinnik, L., L. Breger, and B. Romanowicz (1998), Anisotropic structures at the base of the Earth's mantle, *Nature*, *393*, 564–567.

Walker, K. T., A. A. Nyblade, S. L. Klemperer, G. H. R. Bokelmann, and T. J. Owens (2004), On the relationship between extension and anisotropy: Constraints from shear wave splitting across the East African Plateau, *J. Geophys. Res.*, *109*, B08302, doi:10.1029/2003JB002866.

Wang, Y., and L. Wen (2004), Mapping the geometry and geographic distribution of a very low velocity province at the base of the Earth's mantle, *J. Geophys. Res.*, *109*, B10305, doi:10.1029/2003JB002674.

Wang, Y., and L. Wen (2007), Geometry and P and S velocity structure of the "African Anomaly," *J. Geophys. Res.*, *112*, B05313, doi:10.1029/2006JB004483.

Wen, L. (2000), Intense seismic scattering near the Earth's core-mantle boundary beneath the Comoros hotspot, *Geophys. Res. Lett.*, *27*, 3627–3630.

Wen, L. (2001), Seismic evidence for a rapidly varying compositional anomaly at the base of the Earth's mantle beneath the Indian Ocean, *Earth Planet. Sci. Lett.*, *194*, 83–95.

Wen, L. (2006), A compositional anomaly at the Earth's core-mantle boundary as an anchor to the relatively slowly-moving surface hotspots and as source to the DUPAL anomaly, *Earth Planet. Sci. Lett.*, *246*, 138–148.

Wen, L., P. Silver, D. James, and R. Kuehnel (2001), Seismic evidence for a thermo-chemical boundary layer at the base of the Earth's mantle, *Earth Planet. Sci. Lett.*, *189*, 141–153.

Wookey, J., J. M. Kendall, and G. Barruol (2002), Mid-mantle deformation inferred from seismic anisotropy, *Nature*, *415*, 777–780.

Yardley, G. S., and S. Crampin (1991), Extensive-dilatancy anisotropy: relative information in VSPs and reflection surveys, *Geophys. Prospect.*, *39*, 337–355.

Zhong, S. (2006), Constraints on thermochemical convection of the mantle from plume heat flux, plume excess temperature, and upper mantle temperature, *J. Geophys. Res.*, *111*, B04409, doi:10.1029/2005JB003972.

Y. Wang, CGGVeritas, 10300 Town Park Drive, Houston, TX 77072, USA. (yi.wang@cggveritas.com)

L. Wen, Department of Geosciences, State University of New York at Stony Brook, Stony Brook, NY 11794, USA. (lianxing.wen@sunysb.edu)